Brain Stimulation 13 (2020) 474–483

Contents lists available at ScienceDirect

Brain Stimulation

journal homepage: http://www.journals.elsevier.com/brain-stimulation

Model-driven neuromodulation of the right posterior region promotes encoding of long-term memories

Ivan Alekseichuk [a, b, *, 1], Zsolt Turi [a, 1], Sibel Veit [a], Walter Paulus [a]

[a] Department of Clinical Neurophysiology, University Medical Center Göttingen, Georg-August University of Göttingen, 37075, Göttingen, Germany
[b] Department of Biomedical Engineering, University of Minnesota, Minneapolis, MN, 55455, USA

ARTICLE INFO

Article history:
Received 27 June 2019
Received in revised form
21 November 2019
Accepted 16 December 2019
Available online 19 December 2019

Keywords:
tACS
EEG
fMRI
Long-term memory
Facial memory
Theta rhythm
Parietal cortex

ABSTRACT

Background: Long-term recognition memory depends both on initial encoding and on subsequent recognition processes.
Objective: In this study we aimed at improving long-term memory by modulating posterior parietal brain activity during the encoding process. If this area is causally involved in memory encoding, its facilitation should lead to behavioral improvement. Based on the dual-process memory framework, we also expected that the neuromodulation would dissociate subsequent familiarity-based and recollection-based recognition.
Methods: We investigated the role of the posterior parietal brain oscillations in facial memory formation in three separate experiments using electroencephalography (EEG), functional magnetic resonance imaging (fMRI), and model-driven, multi-electrode transcranial alternating current stimulation (tACS).
Results: Using fMRI and EEG, we confirmed that the right posterior parietal cortex is an essential node that promotes the encoding of long-term memories. We found that single-trial low theta power in this region predicts subsequent long-term recognition. On this basis, we fine-tuned the spatial and frequency settings of tACS during memory encoding. Model-driven tACS over the right posterior brain area augmented subsequent long-term recognition memory and particularly the familiarity of the observed stimuli. The recollection process, and short-term task performance as control remained unchanged. Control stimulation over the left hemisphere had no behavioral effect.
Conclusion: We conclude that the right posterior brain area is crucial in long-term memory encoding.

Introduction

The success and the strength of memory depend on the perpetually changing neural activity from memory encoding to recognition of the encountered stimulus. This neural activity often occurs as oscillations in the theta frequency band. Theta oscillations dominate hippocampal activity, the hub of memory consolidation [1,2], and play a role in the hippocampal-neocortical interactions [3–5] as well as in the neocortical networks [6–8]. It has been suggested that this rhythm reflects local fluctuations of neural state between potentiation and depression [9,10]. Theta rhythm provides temporal organization for memory engrams [11–14], coordinates anatomically distributed nodes of the memory network [15,16], and "glues" associative memories [17,18]. While the mnemonic role of medial-temporal theta oscillations is well established, their function in the parietal lobe remains a matter of debate. On one hand, some studies suggest parietal involvement only during recognition [reviewed by 19,20], whereas other studies indicate its crucial engagement already during encoding [cf. 21–23].

After memory encoding, the active process of remembering results in different intensities of conscious experience. A memory engram can be retrieved with or without fine episodic details that are described by the terms recollection and familiarity, respectively [24–26]. The dual-process memory framework describes recollection as an all-or-nothing process, while familiarity is a distinct continuous process that can recover partial details [27,28]. Neuroanatomical studies indicate that hippocampal and cortico-hippocampal network activities drive recollection, whereas familiarity involves the hippocampus to a lesser degree and engages the distributed neocortical network [29–31].

* Corresponding author. 312 Church St. SE, Minneapolis, MN 55455, USA.
E-mail address: ialeksei@umn.edu (I. Alekseichuk).
[1] These authors contributed equally.

https://doi.org/10.1016/j.brs.2019.12.019

Here, we investigated the role of brain oscillations in memory formation using model-driven, multi-electrode transcranial alternating current stimulation (tACS). It is hypothesized that the application of oscillatory electrical currents can amplify corresponding brain oscillations or rhythms [32,33]. Since brain rhythms play a vital organizational part in neural communications [15,34], tACS enables the investigation of causal links between neural activity and behavior [35]. This is particularly promising for memory research where many phenomena exhibit distinct oscillatory signatures [36].

Recent invasive electrophysiological studies of tACS mechanisms in animals highlight the importance of the brain state and adequate dose calculation for a successful intervention [37–42]. Whereas low intensity stimulation (<0.1 V m^{-1}) [40] or stimulation under anesthesia induce no immediate electrophysiological effects [37,38], higher intensity stimulation (>0.3 V m^{-1}) in awake primates has been shown to reliably modulate ongoing spike timing of single neurons in a frequency-specific manner [39,41]. Therefore, we employed computational modeling to ensure localized stimulation with a sufficient electric field in the parietal brain area of interest (>0.4 V m^{-1}), and we compared target stimulation with placebo and active control conditions. The latter included the stimulation over an area of no interest as a control for anatomical specificity and possible confounders due to activation of the peripheral nervous system [38].

Even at higher doses, it is essential to adjust the stimulation parameters to the brain activity of interest to increase the specificity and effectiveness of tACS [35,43]. In this study, we aimed to establish the generalized profile of memory encoding activity and stimulation settings that represent the common denominator to interact with it. Thus, we fine-tuned the spatial and frequency parameters of tACS using group-level functional neuroimaging and electrophysiological recordings that characterized our memory task [5,35]; and we conducted the imaging, electrophysiological and brain stimulation studies in separate groups of participants with the ambition to better generalize our findings to the population-level.

Our imaging data confirmed that the parietal cortex shows activity during memory encoding in the low theta band. We hypothesized that stimulation with low theta rhythm inducing subsequent behavioral changes would support one of two competing models. In the “attention-to-memory” model [19,20], tACS over the parietal cortex during memory encoding will not impact memory formation because this area is only active during recognition. According to the “reinstatement hypothesis” [21–23], model-driven tACS will boost memory encoding and subsequent recognition because the parietal cortex is already involved in the encoding. Further, we expected that model-driven tACS would dissociate subsequent familiarity-based and recollection-based recognition, if these processes are partially independent as postulated by the dual-process memory framework.

In the present study we found that model-driven tACS during memory encoding augmented subsequent memory performance. Specifically, we observed that the memory boost was due to the increase in familiarity but not in recollection processes. Thus, our findings confirm and extend previous correlative evidence by showing that the right posterior parietal brain region including the parietal cortex is a prime node for encoding long-term memories, particularly supporting subsequent familiarity process. We also demonstrated the feasibility of our strategy of applying model-driven tACS to augment long-term memory. This has implications for both memory research and clinical treatment [44].

Methods

Participants. Sixty-five healthy, adult volunteers participated in this study: 20 volunteers in the EEG experiment (12 female, 18 right-handed, 19–29 years old, 9–23 years of education), 20 volunteers in the fMRI experiment (12 female, 20 right-handed, 18–32 years old, 12–25 years of education), and 25 volunteers in the brain stimulation experiment (13 female, 21 right-handed, 18–28 years old, 13–20 years of education). All participants gave their written informed consent prior to the study, had a normal or corrected-to-normal vision, and underwent basic health screening in which they reported no symptoms or history of traumatic brain injury, substance abuse, chronic neurological, psychiatric, or cardiovascular disorders. All experiments were conducted in accordance with the Declaration of Helsinki, and regulations of the Ethics Committee of the University Medical Center Göttingen, Germany.

Experimental Design. The present investigation encompassed two neuroimaging studies with different modalities (EEG and fMRI), and one brain stimulation study that was based on the neuroimaging findings. All volunteers were familiarized with the task and laboratory environment before the first session, and each participant took part in only one study.

The EEG and fMRI investigations consisted of one initial visit and one experimental session. In the EEG study, the data was recorded in the psychophysiological laboratory, where the volunteer performed the entire task. In the fMRI study, the encoding task block was conducted in the scanner, while long-term recognition was tested outside the scanner in the psychophysiological laboratory.

The brain stimulation study was designed as a double-blinded, placebo-controlled, randomized, counterbalanced crossover experiment with the model-driven parameters derived from the neuroimaging experiments. In addition to the training during the initial visit, all volunteers attended three sessions with the following conditions in a counterbalanced, pseudorandomized order: target stimulation, active control, and placebo control (i.e., sham stimulation). There was a between-session interval of at least 72 h to minimize carry-over effects.

Behavioral Paradigm. Our item base consisted of 918 color photographs of adult human faces (558 female, 360 male) from the online photo gallery of frontal portraits with neutral facial expression (Humanae Project by Angelica Dass,www.angelicadass.com).

Before beginning the experiments, the participants received written and verbal instructions. On a separate day before the experiment, they performed a short familiarization session with 22 stimuli to ensure that they had correctly understood the instructions and were able to operate the computer program. The presentation of the visual stimuli was performed by the PsychoPy [45].

The behavioral paradigm consisted of two tasks that were separated by a delay period of 20 min. In the encoding and short-term memory recognition task, the participants first had to memorize a series of 4, 5 or 6 unfamiliar face-monetary value pairs that had been randomly selected from a total of 90 pairs. We used 45 female and 45 male faces, and each series included only female or male faces. The monetary value is either a negative (range from −150 to −10) or positive (range from 10 to 150) value. It is displayed with the corresponding sign (−/+) directly below each facial stimulus (Arial, 25 pt) and aligned with the center. Each stimulus pair was displayed for 3s followed by the fixation cross for 0.5s. Following a maintenance period of 10s, the participants viewed the same series of faces presented with one correct and one incorrect monetary value. The incorrect monetary value was automatically calculated by randomly adding or extracting values in a range of 5–9 from the correct value. This procedure ensured that

the incorrect value never changed its sign. Both monetary values were displayed directly below each facial stimulus (Arial, 25 pt) and aligned left and right. The presentation order of the stimuli in the short-term recognition phase was randomized. The task of the participants was to choose the correct monetary value for each face in a two-alternative forced choice task. The stimuli were displayed for 3s, during which the participants had to give their answers. Correct answers were counterbalanced between the "left" and "right" decisions. There was no feedback to the volunteer regarding the correctness of their answer. The next stimulus pair was presented after the fixation cross (0.5s). The next series was displayed after a delay interval of 12–16s.

Following a delay period of 20 min after the end of encoding and short-term memory recognition task, the participants performed the long-term memory recognition task. Here, they viewed a total of 180 unfamiliar faces (90 female and 90 male); half of which had already been shown during the encoding task. The participants used a six-point Likert scale in an old-new recognition paradigm to indicate whether they had already seen the face (i.e., it is old) or not (i.e., it is new), as well as their level of confidence (definitely > probably > maybe). The answers thus formed six categories: "definitely old", "probably old", "maybe old", "maybe new", "probably new", and "definitely new". The stimulus was presented until a response was obtained.

EEG Acquisition. EEG data were recorded using a 128-channel amplifier (actiCHamp, BrainVision) with active electrodes (actiCAP, BrainVision), which were attached according to the international 10-05 electrode placement system. All recordings were referenced to the FCz channel. The sampling rate was set to 2 kHz at an analog-digital precision of 24 bits. The impedance was kept below 20 kOhm, and no hardware filters were applied. The EEG amplifier received synchronization triggers from the psychophysiological computer via a TTL parallel connection, which was controlled by the PsychoPy software [45].

MRI Acquisition. MRI data was recorded with a Magnetom Tim Trio 3 T scanner (Siemens™) using a 32-channel phased-array head coil. T1-weighted whole brain anatomical scans were acquired with the 3D turbo fast low angle shot sequence (repetition time: 2250 ms, echo time: 3.26 ms, inversion time: 900 ms, flip angle: 9 deg, isotropic resolution: 1 mm^3). T2*-weighted whole-brain functional scans were obtained with the 2D multiband gradient-echo echo-planar sequence (39 slices per volume, repetition time: 900 ms, echo time: 30 ms, flip angle: 50 deg, in-plane resolution: 3 mm^2, between-slice gap: 10%, multiband acceleration factor: 3, phase coding: anterior > posterior). In addition, short T2*-weighted series were recorded using the same parameters, but with inverse phase coding (posterior > anterior). The memory task was presented to the volunteers in the scanner using a projector and a system of mirrors.

For the purpose of brain stimulation modelling, six scans were acquired, including four anatomical images: two T1-weighted whole brain scans with and without fat suppression (3D turbo fast low angle shot sequence, repetition time: 2250 ms, echo time: 3.26 ms, inversion time: 900 ms, flip angle: 9 deg, isotropic resolution: 1 mm^3); and two T2-weighted whole brain anatomical scans with and without fat suppression (3D turbo spin echo, repetition time: 3500 ms, echo time: 282 ms, flip angle: variable, parallel acquisition technique factor: 2, isotropic resolution: 1 mm^3). Whole brain diffusion tensor images (75 slices, resolution: 1.7 mm^3, repetition time: 10000 ms, echo time: 88 ms, GRAPPA acceleration factor: 2, 6/8 phase partial Fourier) with 64 diffusion directions and a b-value of 1000 S mm^{-2} were collected for estimation of tissue anisotropy. Gradient echo field map sequences (75 slices, resolution: 1.7 mm^3, repetition time: 890 ms, echo time one: 4.92 ms, echo time two: 7.38 ms, flip angle: 70 deg) were recorded and used for DTI distortion correction.

Model-Driven Brain Stimulation. A multi-channel stimulator (StarStim®, Neuroelectrics) with five round, rubber electrodes (r = 1 cm) and Ten20 conductive paste was used in all sessions. Transcranial alternating current stimulation (3 mA peak-to-peak, i.e. 1.5 mA peak-to-zero) was delivered during the learning task block (≈20 min, including ramp-up and ramp-down periods of 10 s) using focal 4x1 montage, warranting homogenous current flow [46]. The placebo stimulation was delivered according to the fade-in/fade-out blinding protocol for 10 s at the beginning and end of the learning task block. The impedance for all electrodes was kept below 10 kOhm.

The stimulation frequency was derived from the results of the EEG experiment and set to 4 Hz. The desired spatial boundaries of the electric field in the brain were defined from the intersection of EEG and fMRI data, and established using the SimNIBS2 modeling framework [47]. The head model of a representative volunteer was generated from the anatomical MRI scans with the routine 'mri2mesh' that engaged the FreeSurfer and FSL functions. Brain tissues anisotropy was estimated from the field map-corrected diffusion tensor images according to the volume-normalized approach. The realistic anisotropic finite element model was comprised of ca. 3 million tetrahedral elements and included five compartments: scalp ($\sigma = 0.25$ S m^{-1}), skull ($\sigma = 0.01$ S m^{-1}), cerebrospinal fluid ($\sigma = 1.79$ S m^{-1}), grey matter ($\sigma_{mean} = 0.276$ S m^{-1}), and white matter ($\sigma_{mean} = 0.126$ S m^{-1}). Virtual stimulation electrodes ($\sigma = 0.1$ S m^{-1}) with the cable connectors and conductive paste ($\sigma = 1$ S m^{-1}) were constructed to capture their actual physical size and were fitted to the scalp locations according to the 10-05 electrode placement system. The following montage was chosen to target the right posterior area (target stimulation condition): the central electrode at P4 versus the return electrodes at T8, C2, CP1, and Oz (each pulled 25% of the current). Mirrored, left hemisphere montage was introduced as an active control condition: the central electrode at P3 versus the return electrodes at T7, C1, CP2, and Oz. The electric field distributions were post-processed and visualized in Gmsh.

Potential side effects and blinding validity were assessed by standardized questionnaires at the end of each session [48]. The volunteer was asked to report the occurrence of phosphenes and unwanted skin sensations on a scale from 0 (none) to 10 (excessive). No volunteer experienced phosphenes. The skin sensation reports indicated 1.52 ± 1.5 points (mean ± SD) for the target stimulation, 1.43 ± 1.3 points for the active control condition, and 1.56 ± 1.5 points for the placebo control condition, with no significant difference between the conditions (Kruskal-Wallis location test $p = 0.94$; Brown-Forsythe variance test $p = 0.61$).

Given the crossover study design, we used Spearman correlation to ensure that pseudo-randomization procedure suppressed possible session order effects. Spearman correlation between the performance in the long-term memory task and the session order is $r = 0.12$, $p = 0.32$; the correlation between the average performance in the short-term memory task and the session order is $r = 0.02$, $p = 0.85$.

The robustness of the statistically significant results was tested using leave-one-out cross-validation (LOOCV) procedure: We systematically left out each subject from a dataset and calculated the statistics in the subsample, which gave 25 iterations. The median statistical estimates across the iterations (p_{LOOCV}) are given in Results.

EEG Analysis. The data were analyzed in MATLAB with the FieldTrip toolbox [49]. Raw recordings were cut on the segments of memory encoding, filtered with an eighth order, forward-reverse Butterworth IIR filter between 0.2 and 45 Hz with an additional

DFT filter at 50 Hz, linearly detrended, and downsampled to 500 Hz. A semi-automatic routine for detecting noisy trials and channels based on the abnormal moments of EEG amplitude was then utilized ('ft_rejectvisual'). An average of four trials per session were excluded, and six channels were marked as noisy and interpolated from the neighboring sensors. The data were re-referenced to the common average and cleaned of blinking artifacts using a independent component analysis (extended InfoMax algorithm). On average, two components were excluded. Overall, 83 of the 1800 trials in the global dataset were excluded, and the median matrix rank decreased from 127 in the raw recordings to 118 in the preprocessed data.

First, we investigated the power differences between the conditions. The time series were normalized and epoched from the appearance of the memory item to 1 s after. Frequency transformation was performed by convolving the signal with the Slepian window function. We examined all frequencies from 1 Hz to 40 Hz with 1 Hz frequency resolution. Epochs that characterized the subsequently recognized (ENC_{HIT}) and forgotten (ENC_{MISS}) memory items were separately averaged within the subjects. They were further interrogated with the group-level, nonparametric, cluster-based permutation test (10,000 iterations, two-tails $p \leq 0.05$, and cluster size $p \leq 0.05$).

Then, we applied linear spatial filtering to the data to increase the signal-to-noise ratio [50]. Identified clusters of significant power differences between the conditions were used to design the filter parameters. Each filter corresponded to one single spatial and frequency cluster:

$$F = \frac{1}{N} \times \left(\sum_{n=1}^{N} w_n \times S_n \right), \quad w_n = \frac{\overline{X}_d^n}{\left(s_d^n / \sqrt{(k-1)} \right)}$$

Where F is the filtered signal, n is the sensor from 1 to N that belongs to the statistical cluster, w is the weight, S is the unfiltered signal, X_d is the average power difference between the conditions for a given frequency, s_d is the standard deviation of those differences, and k is the number of observations, i.e., subjects.

The single individual trials were then projected through two spatial filters (see Fig. 2A) and sorted into six categories depending on the subsequent memory effect (see Fig. 2C and subchapter "Memory Task"). Theta power was estimated per each trial by convolving the time series with the Slepian window function (frequency of interest: 4 Hz, spectral smoothing: 1 Hz), and was further interrogated on the presence of psychophysiological interactions (see subchapter "Psychophysiological Analysis").

To analyze the effective connectivity between the clusters of interest, we used preprocessed and spatially filtered data. The time series were further downsampled to 200 Hz to ensure adequate time resolution for the autoregressive model. It was built with the Vieira-Morf algorithm using unbiased covariance estimates (as implemented in the BioSig routine 'mvar', AR order: 10). The spectrally resolved method from the Granger Causality family – Directed Transfer Function, was applied to reveal the presence and dominant direction of frequency-specific connectivity. The entire EEG spectrum (1–40 Hz) was analyzed. First, the presence of significant connectivity was examined with the nonparametric permutation test. The parameters of spatial filters (namely, sensor locations and weights) were randomly permuted 10,000 times to calculate the "dummy" distribution of DTF values. The confidence interval (99%) of this distribution was taken as the significance threshold and compared with the DTF values from the real data. Second, the dominant direction of the connectivity was examined employing a cluster-corrected Wilcoxon rank-sum test (two-tailed $p \leq 0.05$). The DTF values that described the opposing directions were compared per each frequency bin, and significant adjacent frequency bins were grouped into the frequency clusters. The cluster-level significance was controlled by the permutation test (10,000 iterations, two-tailed $p \leq 0.05$, FDR corrected for the number of frequency clusters). Both the statistically significant presence of connectivity and evidence for its dominant direction were required to reach a conclusion.

MRI Analysis. Raw DICOM images were converted into the NIfTI format with SPM. Geometric distortions in the echo planar images were estimated for every session by creating the field map with the FSL routine 'topup' and calculating on its basis the voxel displacement map in the FieldMap SPM toolbox. The remaining preprocessing, denoising, and data analysis was performed in the functional connectivity toolbox (CONN). The details of this framework are given elsewhere [51].

The preprocessing started with the realignment of the functional images to the first volume utilizing the rigid body spatial transformation, followed by the unwarping and distortion correction according to the voxel displacement map, and slice timing correction. ART-based outlier detection was then performed (the global signal z-value threshold was set to 3 and subject motion threshold – to 0.5 mm). Brain volumes were segmented into grey matter, white matter, and cerebrospinal fluid, and normalized to the MNI space. Functional images were smoothed with 8 mm full-width-at-half-maximum Gaussian kernel. Finally, all outliers were scrubbed, and the component-based noise correction was performed (the 'aCompCor' method). The motion parameters with their first order temporal derivatives, the white matter and CSF related principal components (five each) were regressed out of the BOLD signal. Data were linearly detrended and bandpass-filtered from 0.008 to 0.1 Hz. Neuroanatomical regions of interest (ROI) were defined according to the Harvard-Oxford atlas (91 cortical and 14 subcortical ROI, covering the whole brain except the cerebellum and brainstem).

We investigated the generalized psychophysiological interactions (gPPI) with focus on the encoding events, which were sorted into two conditions: the subsequently recognized (ENC_{HIT}) and forgotten (ENC_{MISS}) items. Given the nature of the long-term memory task, six ROI were taken as the connectivity seeds: left and right hippocampus, and left and right anterior and posterior parahippocampal gyri. Seed-to-ROI analyses was performed to estimate the joint effect of both conditions (F-test). The general linear model was implemented to examine the statistical significance (two-tails $p \leq 0.05$, FDR corrected for the number of seed-to-ROI links). F-statistics, beta regression coefficients, and corrected p-values are reported in the results section.

In the *post hoc* test, the single connectivity seed was placed in the right angular gyrus, while all other settings were the same as above.

Psychophysiological Analysis: EEG. The relationships between the single trial theta power during the memory encoding (in power units) from one side and subsequent memory effect (six categories) or subsequent decision time (in seconds) from the other side were interrogated with the generalized linear model. The single trial theta power was estimated separately for each significant cluster (see subchapter "EEG Analysis"), which gave one predictor variable per cluster. F-statistics, degrees of freedom, and p values are reported in the results section. In addition, the monotonic correlation between the subsequent decision time and the single trial theta power during the memory encoding was estimated as the Spearman coefficient. To determine whether the short-term recognition predicted the subsequent memory effect, we used the linear regression function.

The agreement of theta power distributions with the single-process or dual-process memory models was interrogated with

linear regression analysis. For that, the median power values, which were calculated per category of the subsequent memory effect, were loaded into the linear model in two different orders. The single-process model predicts that the single-trial theta power should be distributed linearly across the six categories from the highest values for subsequent confident recognitions to the lowest values for the unconfident mistakes as following: 'very confident correct choice' > 'less confident correct choice' > 'unconfident correct choice' > 'unconfident wrong choice' > 'more confident wrong choice' > 'very confident wrong choice'. On the contrary, the dual-process model assumes that the confidence and correctness are different dimensions, thus, 'correct choice' > 'wrong choice' and 'very confident choice' > 'less confident choice' > 'unconfident choice'. These relations would result in a V-shaped distribution of theta power, with the highest power allocated for high confidence hits, high theta power for high confidence misses and the lowest power for low confidence recognition categories and particularly for low confidence misses. The model fitting was done with the ordinary least squares method. T-statistics for the slope parameters, degrees of freedom, p values, and adjusted R^2 are reported in the result section.

Psychophysiological Analysis: Brain Stimulation. The impact of brain stimulation during memory encoding was tested using the generalized linear mixed-effect model (GLMM), specified as following: 'response variable ~ 1 + stimulation condition + (1 | participant id)'. Raw performance and confidence during the long-term recognition task, and performance in the short-term recognition task were used as the response variables (in three separate models, respectively), while the stimulation condition was used as the fixed effect variable. The participant id was coded as the random effect variable to factor for the interindividual differences. F-statistics, degrees of freedom, and p values regarding the fixed effect factor are reported in the result section. *Post hoc*, when GLMM demonstrated significant effect, the nonparametric Wilcoxon signed-rank test (two-tailed $p \leq 0.05$) was used for pairwise comparisons between the stimulation conditions. The effect sizes for every significant comparison are given in Hedges' g with 90% confidence intervals. Hedges' g is a robust, unbiased version of Cohen's d estimator, which can be interpreted in the same way.

The dual-process signal detection model (DPSD) was implemented to estimate the strength of familiarity and recollection of the memory items during the long-term recognition task. Details of the model are given elsewhere [28]. In short, the model assumes that two different processes support recognition of the stimulus: precise recollection of items in full detail from the memory (mathematically described as a high threshold model with recollection of oldness (R_O) as a free parameter) and, when recollection is not achieved, the familiarity assessment (a signal detection model with the mean of familiarity (d_F) as a free parameter and variance of familiarity as a constrained parameter). The constrained DPSD model predicts the cumulative proportion of old and new items in each rating bin (B_i represents a volunteer's choice in the task) with the decision boundaries in-between (c_k) by fitting the following formulations into the data with the maximum likelihood method:

$$\begin{cases} p(B_i|''Old'') = R_O + (1 - R_O)\Phi[c_k - d_F, 1] \\ p(B_i|''New'') = \Phi[c_k, 1] \end{cases}$$

Where Φ denotes the Gaussian cumulative distribution function [mean, standard deviation]. The model parameters (familiarity and recollection) were compared between the stimulation conditions with the nonparametric Wilcoxon signed-rank test (two-tailed $p \leq 0.05$). Where appropriate, the effect sizes are given as Hedges' g with 90% confidence intervals.

Results

We first studied the neural characteristics of the subsequent long-term memory effect by electroencephalography (EEG) and functional magnetic resonance imaging (fMRI). In two separate experiments, participants performed the multi-stage memory paradigm that encompassed encoding and short-term recognition, maintenance, and long-term recognition tasks (Fig. 1).

In the EEG experiment, two significant clusters of difference between the encoding of subsequently recognized vs. missed items emerged from the full range (1–40 Hz), nonparametric, cluster-corrected permutation test between the categories (Fig. 2A, $p_{sensor} \leq 0.05$ and $p_{cluster} \leq 0.05$). The clusters are localized in the right posterior ($T_{peak}(19) = 4.63$) and the mid/left frontal regions ($T_{peak}(19) = 3.62$) with frequencies in the low theta to high delta range (4 ± 1 Hz). The full EEG spectrum can be seen in the Supplementary material (Fig. S1). Low theta frequency (4 Hz) entered the tACS experiment as the targeted stimulation frequency.

Next, we examined the single-trial low theta (θ) power relative to the six behavioral categories of subsequent recognition success (hit or miss) and confidence levels (definitely > probably > maybe)

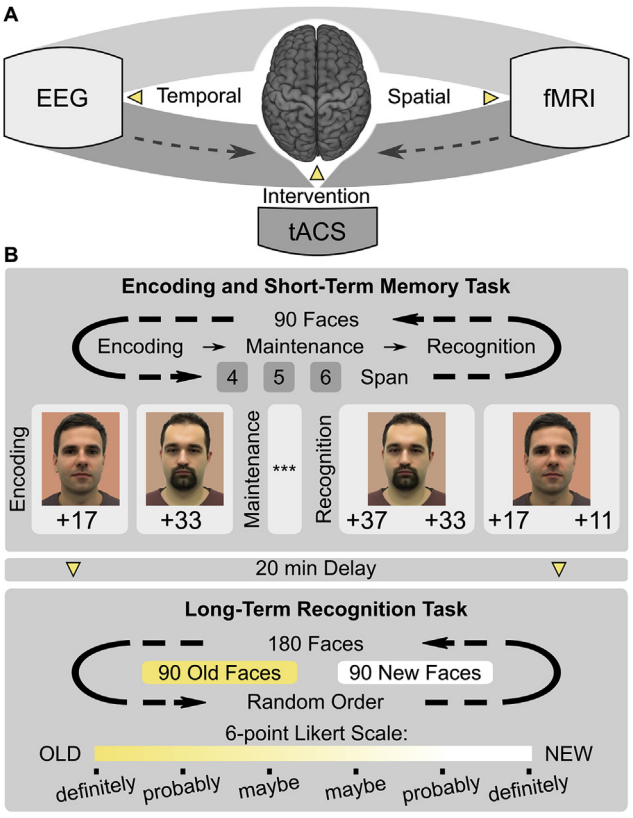

Fig. 1. General procedure and behavioral paradigm.
(A) Electroencephalogram (EEG) and functional magnetic resonance imaging (fMRI) are acquired during the encoding task in the experiments 1 and 2. The resulting spatial and oscillatory features of the subsequent memory effect were combined into a model-driven transcranial alternating current stimulation (tACS) protocol in experiment 3.
(B) The behavioral paradigm consisted of two consecutive tasks. In the encoding and short-term memory recognition task, participants were requested to memorize a series of 4, 5, or 6 unfamiliar face and monetary value pairs. Following a maintenance period of 10 s, the participants were required to choose the monetary value corresponding to each face in the two-alternative forced choice task (no feedback was provided about the decision correctness). In the long-term memory recognition task, the participants viewed 180 faces (90 new) and used a six-point Likert scale to indicate whether they had already seen the face or not, as well as their level of confidence in their choice (definitely > probably > maybe).

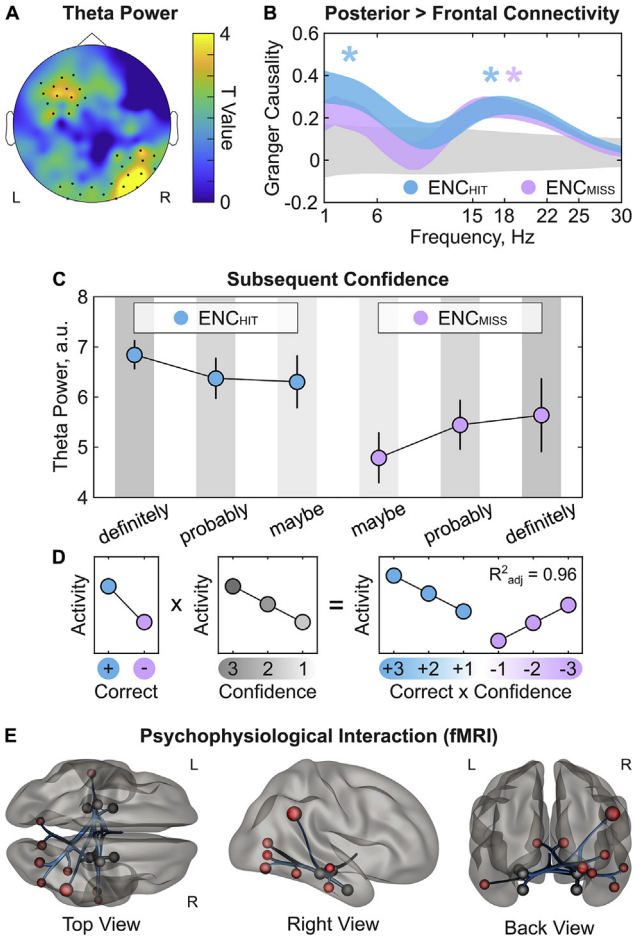

Fig. 2. Functional signature of the subsequent memory effect.
Panels A–C correspond to the EEG and panel F – to the fMRI analysis. (A) Frequency analysis revealed significant ($p_{corr} \leq 0.05$) increases in theta power in the frontal and right posterior cortices. See Figs. S1–2 for more data. (B) The Granger Causality between the spatially filtered signals from the posterior to frontal region minus the opposite direction (median ± pooled variance). The grey curve corresponds to the null distribution ±99% confidence interval. (C) The single-trial theta power (±SEM) in the right posterior cluster during memory encoding in relation to the correct subsequent recognition (ENC_{HIT}) or miss (ENC_{MISS}). (D) The single trial theta power is organized according to the dual-process memory model, which assumes that response correctness and confidence exist in independent dimensions. (E) Generalized psychophysiological interaction analysis of the subsequent memory effect. Black spheres correspond to the ad hoc connectivity seeds in the para-/hippocampus. Red spheres correspond to the identified regions-of-interest ($p_{corr} \leq 0.05$).

(Fig. 2C). The generalized linear model (GLM) confirmed that the single-trial theta power is a biomarker that predicts the subsequent decision in the *long-term* memory task. In the joint statistical model ('memory performance ~ 1 + right posterior θ + frontal θ'), the right posterior but not the frontal theta cluster was significant (Right posterior θ: $F_{(1,1714)} = 4.47$, $p = 0.035$; Frontal θ: $F_{(1,1714)} = 1.44$, $p = 0.23$). Moreover, we found a significant linear relationship between the individual long-term memory performance and individual θ power during memory encoding at 4 ± 1 Hz ($R^2_{adj} = 0.54$, $p_{corr} = 0.0007$), which was not the case for the neighboring frequencies (namely, 3, 5, 6, and 7 ± 1Hz; all $p > 0.2$). For details, see Supplementary Fig. S2. The decision time during face recognition was negatively proportional to the theta power as reveled by GLM (Right posterior θ: $F_{(1,1714)} = 21.35$, $p = 4.1 \times 10^{-6}$; Frontal θ: $F_{(1,1714)} = 0.1$, $p = 0.75$) and Spearman correlation (Right posterior θ: $r = -0.17$, $p = 5.5 \times 10^{-12}$; Frontal θ: $r = -0.12$, $p = 6.3 \times 10^{-7}$). At the same time, the analysis showed no link of *short-term* memory performance to single-trial theta activity in the clusters of interest (Right posterior θ: $F_{(1,1702)} = 2.58$, $p = 0.11$; Frontal θ: $F_{(1,1702)} = 0.02$, $p = 0.88$). We also observed no linear relationships between the short-term and long-term memory performances (1787 trials, $R^2_{adj} = 3.1 \times 10^{-4}$, $p = 0.21$), which indicates their functional independence. Thus, the single-trial theta power in the right posterior region is crucial for encoding *long-term* memories, but it does not affect short-term recognition memory.

The distribution of single-trial low theta power during the encoding along six categories of subsequent behavior demonstrates a statistical pattern. The low theta power monotonically decreases from higher to lower confidence categories of subsequent decisions and, independently, it is higher for the subsequent recognition than for miss (Fig. 2C and D). This distribution supports the dual-process model of recognition memory (fit into the data: $R^2_{adj} = 0.96$, $p = 4.6 \times 10^{-4}$) over the single-process model ($R^2_{adj} = 0.43$, $p = 0.09$), the latter of which would expect a continuous monotonic function along all six categories.

Finally, we interrogated the causality between the right posterior and frontal activity after spatial filtering employing the frequency-resolved Granger Causality [52]. Nonparametric, cluster-corrected permutation tests ($p_{frequency} \leq 0.05$ and $p_{cluster} \leq 0.05$) indicate a (i) significant transfer of information between the two areas during the memory encoding, (ii) posterior-to-frontal direction of the information flow that appeared in the delta-theta (1–6 Hz) and beta (15–25 Hz) bands, and (iii) diminishing information flow in the delta-theta band during the memory encoding of subsequently forgotten faces (Fig. 2B). Noteworthy, the beta band connectivity remains active during the encoding of all stimuli, subsequently remembered and forgotten, possibly reflecting attention or general sensory processing [15] rather than successful long-term binding of the memory engram. All these findings support the role of right-sided posterior parietal theta activity in forming long-term memories.

In the fMRI experiment, we implemented a generalized psychophysiological interactions analysis [53] with *a priori* connectivity seeds in para-/hippocampal regions, which is a crucial hub in memory formation [54,55]. The analysis of encoding epochs revealed the network of brain regions whose association covaries with subsequent recognition (Fig. 2E and Table S1). Activity in the right angular gyrus shows the highest explained variance ($\beta = 1.21$, $F_{(12,8)} = 29.84$, $p_{FDR} = 0.003$) followed by the activity in the occipital and temporal cortices ($0.01 < p_{FDR} < 0.05$). To support the relevance of the right angular gyrus for long-term memory formation, we performed a *post hoc* analysis with the connectivity seed placed there (Table S2). The two most connected regions are the left anterior parahippocampal gyrus and the left hippocampus (both $p_{FDR} = 0.001$). Thus, concordant with the EEG experiment, fMRI indicated that the right angular gyrus was the crucial neocortical hub of long-term face encoding. Furthermore, the results of the EEG and fMRI experiments are in agreement with previous neuroimaging and electrophysiological studies, which highlight the broad brain networks that are involved in the encoding of long-term facial memories including the prefrontal, medial-temporal, inferior temporal and parietal regions [20,56–58].

In the final, brain stimulation experiment, we fused the frequency information from the EEG and the spatial information from the fMRI experiments into a model-driven tACS protocol (4 Hz, 3 mA p-to-p, 4x1 electrode montage). We targeted the right posterior neocortex (target stimulation), the left posterior neocortex (active control), or delivered sham stimulation either to the left or the right posterior neocortex (placebo control) during the encoding and short-term memory task.

The realistic model of the electric field estimated consistent values above 0.4 V m^{-1} and up to 0.8 V m^{-1} in the posterior parietal

neocortex for both target and control stimulations (Fig. 3A). Oscillating electric fields at 0.3 V m^{-1} or higher can induce immediate electrophysiological effects, e.g., modulate spike timing activity of single neurons [39,41]. None of our participants reported experiencing phosphenes during stimulation, but they did report a mild to moderate degree of transient skin sensations, which did not differ across the stimulation conditions (nonparametric ANOVA $p = 0.99$, more details in Methods).

The stimulation experiment confirmed the model-driven prediction about the mnemonic role of right posterior theta rhythm in long-term memory formation. Stimulation during the encoding affected long-term (Fig. 3B–F; $F_{(2,13497)} = 4.73$, $p = 0.009$), but not short-term recognition performance (Fig. S4; $F_{(2,6704)} = 0.36$, $p = 0.7$) according to the generalized linear mixed effect model (GLMM; 'memory performance ~ 1 + stimulation condition + (1 | participant)'). The stimulation effect was further interrogated using *post hoc* nonparametric two-tailed tests. Compared to placebo stimulation, target stimulation significantly improved the overall subsequent long-term memory effect (Fig. 3E; $p = 0.023$, $p_{LOOCV} = 0.028$, effect size Hedges' g [with 90% CI] = 0.34 [0.08 0.59]). No significant effects were observed for the active control condition relative to placebo ($p = 0.48$). Individual performance data are given in the Supplementary material (Fig. S3). In addition, the stimulation had no effect on the decision confidence itself, irrespective of the correctness (Fig. 3F, GLMM $F_{(2,13497)} = 1.73$, $p = 0.18$).

To gain a detailed view of the familiarity and recollection processes, we performed computational modeling of the long-term recognition using the dual-process signal detection framework [25,28]. Target stimulation over the right posterior cortex improved familiarity of the memorized items both relative to the sham stimulation ($p = 0.032$, $p_{LOOCV} = 0.043$, Hedges' $g = 0.41$ [0.05 0.77]) and to the active control condition (Fig. 3B; $p = 0.04$, $p_{LOOCV} = 0.043$, Hedges' $g = 0.41$ [0.08 0.75]). Recollection remained unaffected by the target stimulation (Fig. 3C; $p = 0.69$). The active control stimulation did not differ significantly from placebo in any parameter (familiarity: $p = 0.8$, recollection: $p = 0.09$).

Discussion

In three consecutive experiments using converging approaches, we showed that: (1) the right posterior parietal cortex is crucial for long-term memory encoding; (2) low theta oscillations in this node reflect encoding activity on the single-trial level; (3) model-driven stimulation of the right posterior cortex during encoding improves subsequent familiarity but not recollection.

Our EEG and fMRI results both indicated that the right posterior parietal brain area is an essential node for encoding long-term memory. Furthermore, the model-driven tACS results showed that the electrical stimulation of the right but not the left posterior brain region during encoding improved subsequent recognition by particularly enhancing the familiarity process. Mechanistically, we suppose that the alternating current facilitated the synchronization in the parietal neuronal population [39,41] and dependent neural communications [16,59]. The increased degree of neural synchrony likely improved feature binding during encoding and made the stimulus more familiar at the next encounter. From a physiological perspective, the temporal context theory of recognition memory suggests that when an episode is recalled, it requires the reinstatement of the neural context at the time of memory encoding [60]. This reinstatement is called the neural contiguity effect, recently observed in the human medial-temporal lobe for strong recollection [61]. However, if not remembered, an opposing neural

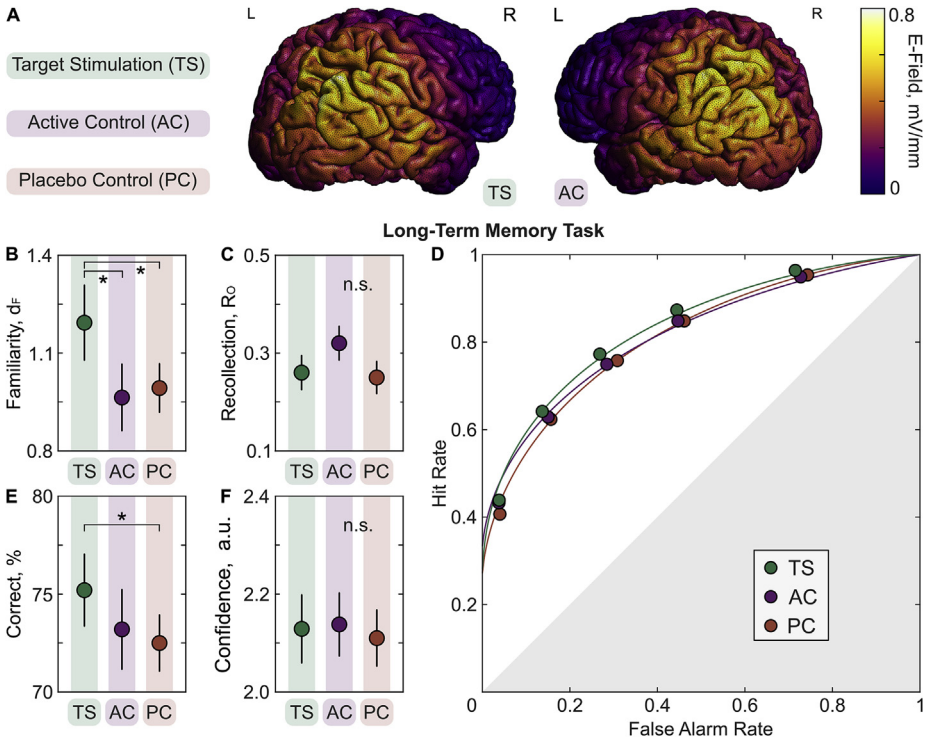

Fig. 3. Transcranial Alternating Current Stimulation.
(A) The electric field distribution on the brain surface during the target and control stimulations (both at 3 mA p-to-p). (B) Familiarity (dF, equivalent to d-prime) of retrieved memories according to the dual-process signal detection framework (here and below, mean ± SEM). (C) Recollection strength (Ro) of memory retrieval. The significance is defined according to GLMM and post hoc nonparametric two-tailed test (*$p \leq 0.05$ for both). (D) Receiver-operating characteristic (ROC) curves of long-term recognition. (E) The overall percent of correct responses in the long-term memory task. See Fig. S3 for individual data. (F) The overall confidence of the choices in the long-term task irrespectively of their correctness.

process takes place in the same anatomical structure, which is called the anti-contiguity effect [61]. If only the memory episode is recovered without its details, the neuronal dissimilarity between encoding and recognition increases. Because in our experiment, the model-driven tACS did not influence the high confidence recollections, it is unlikely that the behavioral improvement is due to directly facilitating the future neural contiguity effect. That might require stimulating the medial-temporal lobe responsible for high confidence recollection memory storage [62,63], but this is hardly feasible using the current non-invasive technologies. Instead, we conclude that the parietal stimulation increased item familiarity by rescuing memories from future anti-contiguity effects. These neural contiguity-like effects should also involve the whole memory-encoding network, including the neocortical right parietal lobe, which can be targeted by model-driven tACS in humans. At the same time, our behavioral findings might have been either caused by directly affecting the neural activity in the posterior brain area including the parietal cortex or by indirectly affecting the medial-temporal lobe via the cortical-hippocampal brain network [5]. Nevertheless, both scenarios are in line with the hypothesis that the parietal cortex is part of the encoding network, which represents the mnemonic information [21]. These findings challenge the "attention-to-memory" model, which assigns a content-independent, top-down role to the parietal cortex for memory recognition [19,20].

Here we demonstrated that the improvement in long-term memory encoding induced by the parietal tACS is selectively driven by the subsequent familiarity process. This pattern of results supports the dual-process view [24,25] on familiarity and recollection. The present findings show that target stimulation helped to distinguish the previously presented from the unseen stimuli (faces). At the same time, target stimulation did not change the recollection process or decision confidence; hence, we argue that the cognitive or behavioral strategy remains the same. It is reasonable to conclude that parietal theta rhythm facilitates the processing of the memory information without playing a significant role in the formation of holistic memory engrams (i.e., engrams with fine episodic details) [31] and metacognition of memory [64], which are probably the prerogative of the hippocampal [31] and frontal networks [64], respectively.

Regarding alternative explanations for our results, one could argue that the model-driven brain stimulation affects long-term but not short-term memory because the latter task requires less cognitive effort. Following such an argument, it implies that the stimulation should be more effective for six-span than for four-span short-term memory blocks, as the former are more challenging. However, this is not the case (Fig. S4), even despite the equivalent level of performance in the six-span short-term memory task as in the long-term memory task ($\approx$70–80%). Another potential argument is that the target stimulation during the encoding phase improves the general attention or arousal rather than mnemonic processes, which as well affects subsequent long-term recognition performance. However, enhanced attention should also affect at least the higher span short-term memory blocks, which again was not the case. Moreover, we found no statistical association between the subsequent recognition of the faces and monetary values presented together during the same encoding trials (correlation $\phi = -0.006$, $p = 0.64$). The latter also argues against a possible improvement of association learning *per se*. Thus, we attribute the behavioral improvement during the target stimulation to the specific augmentation of long-term mnemonic processes.

The present findings raise several questions for the future. Although this study explicitly assesses the long-term memory using the face stimuli, it is plausible that the effects extend to a broader domain of long-term memory. Future research into the selectivity of the right parietal tACS effects for different tasks and stimuli (e.g., visual-spatial tasks) will establish the full scope of the practical value of proposed stimulation. It should be noted that the present focus on the theta rhythm during the memory encoding is based on the EEG experiment, as in the subsequent tACS study we controlled the anatomical but not frequency specificity. Follow-up work with a range of stimulation frequencies, including neighboring faster and slower frequencies [65], could generate additional insights. Another important advance would be to obtain direct electrophysiological recordings during stimulation. While fundamental *in vivo* studies of the tACS mechanisms provide the working understanding of how transcranial electric current reaches the brain [66,67] and affect neurons [33,39], immediate recordings during the memory task could reveal important nuances. The non-invasive methods for such recordings are currently under active development and discussion [68–71], however invasive experiments could be necessary. It is noteworthy that in this study we demonstrated memory improvement in healthy adults. The same interventions in people with memory decline could show greater benefits [72]. Finally, further exploration of dose regimes and multi-session stimulation might lead to an increase in effect size and bring model-driven tACS into the clinical practice.

In summary, using EEG, fMRI, and model-driven tACS, we found that the right posterior parietal region plays a larger, causal role in long-term memory encoding than hitherto assumed. Model-driven tACS in the right posterior region augmented long-term memory performance by particularly enhancing the familiarity process. These findings provide novel support for the "reinstatement model" and the dual-process view of human encoding and recognition. In the clinical context, model-driven tACS has the promise to rescue memory encoding in patients with memory deficits, which calls for further investigation.

Authors contributions

I.A. and Z.T. conceptualized the study; W.P. supervised the study; Z.T. and S.V. prepared the task; I.A. and S.V. collected the data; I.A. analyzed the data; I.A. and Z.T. prepared the figures; I.A., Z.T., S.V., and W.P. wrote the manuscript.

Acknowledgments

We would like to thank Prof. Andrea Antal for her support and Prof. Thomas Crozier for his comments on the manuscript. This research was financially supported by DFG PA 419/15-1. W.P. serves on the scientific advisory board of Precisis AG and holds a patent on transcranial deep-brain stimulation. Other authors declare no competing interests.

Appendix A. Supplementary data

Supplementary data to this article can be found online at https://doi.org/10.1016/j.brs.2019.12.019.

References

[1] Buzsáki G. Theta oscillations in the Hippocampus. Neuron 2002;33:325–40. https://doi.org/10.1016/S0896-6273(02)00586-X.
[2] Buzsáki G, Moser EI. Memory, navigation and theta rhythm in the hippocampal-entorhinal system. Nat Neurosci 2013;16:130–8. https://doi.org/10.1038/nn.3304.
[3] Sirota A, Montgomery S, Fujisawa S, Isomura Y, Zugaro M, Buzsáki G. Entrainment of neocortical neurons and gamma oscillations by the hippocampal theta rhythm. Neuron 2008;60:683–97. https://doi.org/10.1016/j.neuron.2008.09.014.

[4] Hanslmayr S, Staresina BP, Bowman H. Oscillations and episodic memory: addressing the synchronization/desynchronization conundrum. Trends Neurosci 2016;39:16–25. https://doi.org/10.1016/j.tins.2015.11.004.

[5] Wang JX, Rogers LM, Gross EZ, Ryals AJ, Dokucu ME, Brandstatt KL, et al. Targeted enhancement of cortical-hippocampal brain networks and associative memory. Science 2014;345(80):1054–7. https://doi.org/10.1126/science.1252900.

[6] Alekseichuk I, Pabel SC, Antal A, Paulus W. Intrahemispheric theta rhythm desynchronization impairs working memory. Restor Neurol Neurosci 2017;35:147–58. https://doi.org/10.3233/RNN-160714.

[7] Polanía R, Nitsche MA, Korman C, Batsikadze G, Paulus W. The importance of timing in segregated theta phase-coupling for cognitive performance. Curr Biol 2012;22:1314–8. https://doi.org/10.1016/j.cub.2012.05.021.

[8] Violante IR, Li LM, Carmichael DW, Lorenz R, Leech R, Hampshire A, et al. Externally induced frontoparietal synchronization modulates network dynamics and enhances working memory performance. eLife 2017;6:e22001. https://doi.org/10.7554/eLife.22001.

[9] Fell J, Axmacher N. The role of phase synchronization in memory processes. Nat Rev Neurosci 2011;12:105–18. https://doi.org/10.1038/nrn2979.

[10] Colgin LL. Mechanisms and functions of theta rhythms. Annu Rev Neurosci 2013;36:295–312. https://doi.org/10.1146/annurev-neuro-062012-170330.

[11] Lisman J, Jensen O. The theta-gamma neural code. Neuron 2013;77:1002–16. https://doi.org/10.1016/j.neuron.2013.03.007.

[12] Rutishauser U, Ross I, Mamelak A, Schuman E. Human memory strength is predicted by theta-frequency phase-locking of single neurons. Nature 2010;464:903–7. https://doi.org/10.1038/nature08860.

[13] Alekseichuk I, Turi Z, Amador de Lara G, Antal A, Paulus W. Spatial working memory in humans depends on theta and high gamma synchronization in the prefrontal cortex. Curr Biol 2016;26:1513–21. https://doi.org/10.1016/j.cub.2016.04.035.

[14] Turi Z, Alekseichuk I, Paulus W. On ways to overcome the magical capacity limit of working memory. PLoS Biol 2018;16:e2005867. https://doi.org/10.1371/journal.pbio.2005867.

[15] Siegel M, Donner TH, Engel AK. Spectral fingerprints of large-scale neuronal interactions. Nat Rev Neurosci 2012;13:121–34. https://doi.org/10.1038/nrn3137.

[16] Fries P. Rhythms for cognition: communication through coherence. Neuron 2015;88:220–35. https://doi.org/10.1016/j.neuron.2015.09.034.

[17] Clouter A, Shapiro KL, Hanslmayr S. Theta phase synchronization is the glue that binds human associative memory. Curr Biol 2017;27:3143–8. https://doi.org/10.1016/j.cub.2017.09.001. e6.

[18] Lang S, Gan LS, Alrazi T, Monchi O. Theta band high definition transcranial alternating current stimulation, but not transcranial direct current stimulation, improves associative memory performance. Sci Rep 2019;9:8562. https://doi.org/10.1038/s41598-019-44680-8.

[19] Cabeza R, Ciaramelli E, Olson IR, Moscovitch M. The parietal cortex and episodic memory: an attentional account. Nat Rev Neurosci 2008;9:613–25. https://doi.org/10.1038/nrn2459.

[20] Sestieri C, Shulman GL, Corbetta M. The contribution of the human posterior parietal cortex to episodic memory. Nat Rev Neurosci 2017;18:183–92. https://doi.org/10.1038/nrn.2017.6.

[21] Lee H, Kuhl B. Reconstructing perceived and retrieved faces from activity patterns in lateral parietal cortex. J Neurosci 2016;36:6069–82. https://doi.org/10.1523/JNEUROSCI.4286-15.2016.

[22] Brodt S, Gais S, Beck J, Erb M, Scheffler K, Schönauer M. Fast track to the neocortex: a memory engram in the posterior parietal cortex. Science 2018;362(80):1045–8. https://doi.org/10.1126/science.aau2528.

[23] Xue G. The neural representations underlying human episodic memory. Trends Cogn Sci 2018;22:544–61. https://doi.org/10.1016/j.tics.2018.03.004.

[24] Yonelinas AP. The nature of recollection and familiarity: a review of 30 Years of research. J Mem Lang 2002;46:441–517. https://doi.org/10.1006/jmla.2002.2864.

[25] Wixted JT. Dual-process theory and signal-detection theory of recognition memory. Psychol Rev 2007;114:152–76. https://doi.org/10.1037/0033-295X.114.1.152.

[26] Bastin C, Besson G, Simon J, Delhaye E, Geurten M, Willems S, et al. An Integrative Memory model of recollection and familiarity to understand memory deficits. Behav Brain Sci 2019. https://doi.org/10.1017/S0140525X19000621.

[27] Yonelinas AP, Aly M, Wang W-C, Koen JD. Recollection and familiarity: examining controversial assumptions and new directions. Hippocampus 2010;20:1178–94. https://doi.org/10.1002/hipo.20864.

[28] Koen JD, Barrett FS, Harlow IM, Yonelinas AP. The ROC Toolbox: a toolbox for analyzing receiver-operating characteristics derived from confidence ratings. Behav Res Methods 2017;49:1399–406. https://doi.org/10.3758/s13428-016-0796-z.

[29] Smith CN, Wixted JT, Squire LR. The Hippocampus supports both recollection and familiarity when memories are strong. J Neurosci 2011;31:15693–702. https://doi.org/10.1523/JNEUROSCI.3438-11.2011.

[30] Rugg MD, Vilberg KL. Brain networks underlying episodic memory retrieval. Curr Opin Neurobiol 2013;23:255–60. https://doi.org/10.1016/j.conb.2012.11.005.

[31] Horner AJ, Bisby JA, Bush D, Lin W, Burgess N. Evidence for holistic episodic recollection via hippocampal pattern completion. Nat Commun 2015;6:7462. https://doi.org/10.1038/ncomms8462.

[32] Polanía R, Nitsche MA, Ruff CC. Studying and modifying brain function with non-invasive brain stimulation. Nat Neurosci 2018;21:174–87. https://doi.org/10.1038/s41593-017-0054-4.

[33] Liu A, Vöröslakos M, Kronberg G, Henin S, Krause MR, Huang Y, et al. Immediate neurophysiological effects of transcranial electrical stimulation. Nat Commun 2018;9:5092. https://doi.org/10.1038/s41467-018-07233-7.

[34] Singer W. Neuronal oscillations: unavoidable and useful? Eur J Neurosci 2018;48:2389–98. https://doi.org/10.1111/ejn.13796.

[35] Thut G, Bergmann TO, Fröhlich F, Soekadar SR, Brittain J-S, Valero-Cabré A, et al. Guiding transcranial brain stimulation by EEG/MEG to interact with ongoing brain activity and associated functions: a position paper. Clin Neurophysiol 2017;128:843–57. https://doi.org/10.1016/j.clinph.2017.01.003.

[36] Hanslmayr S, Axmacher N, Inman CS. Modulating human memory via entrainment of brain oscillations. Trends Neurosci 2019. https://doi.org/10.1016/j.tins.2019.04.004.

[37] Vöröslakos M, Takeuchi Y, Brinyiczki K, Zombori T, Oliva A, Fernández-Ruiz A, et al. Direct effects of transcranial electric stimulation on brain circuits in rats and humans. Nat Commun 2018;9:483. https://doi.org/10.1038/s41467-018-02928-3.

[38] Asamoah B, Khatoun A, Mc Laughlin M. tACS motor system effects can be caused by transcutaneous stimulation of peripheral nerves. Nat Commun 2019;10:266. https://doi.org/10.1038/s41467-018-08183-w.

[39] Krause MR, Vieira PG, Csorba BA, Pilly PK, Pack CC. Transcranial alternating current stimulation entrains single-neuron activity in the primate brain. Proc Natl Acad Sci 2019. https://doi.org/10.1073/pnas.1815958116.

[40] Lafon B, Henin S, Huang Y, Friedman D, Melloni L, Thesen T, et al. Low frequency transcranial electrical stimulation does not entrain sleep rhythms measured by human intracranial recordings. Nat Commun 2017;8:1199. https://doi.org/10.1038/s41467-017-01045-x.

[41] Johnson L, Alekseichuk I, Krieg J, Doyle A, Yu Y, Vitek J, et al. Dose-dependent effects of transcranial alternating current stimulation on spike timing in awake nonhuman primates. BioRxiv 2019. https://doi.org/10.1101/696344.

[42] Alekseichuk I, Mantell K, Shirinpour S, Opitz A. Comparative modeling of transcranial magnetic and electric stimulation in mouse, monkey, and human. Neuroimage 2019;194:136–48. https://doi.org/10.1016/j.neuroimage.2019.03.044.

[43] Bikson M, Rahman A. Origins of specificity during tDCS: anatomical, activity-selective, and input-bias mechanisms. Front Hum Neurosci 2013;7. https://doi.org/10.3389/fnhum.2013.00688.

[44] Weigelt S, Koldewyn K, Kanwisher N. Face identity recognition in autism spectrum disorders: a review of behavioral studies. Neurosci Biobehav Rev 2012;36:1060–84. https://doi.org/10.1016/j.neubiorev.2011.12.008.

[45] Peirce JW. Generating stimuli for neuroscience using PsychoPy. Front Neuroinf 2009;2. https://doi.org/10.3389/neuro.11.010.2008.

[46] Dmochowski JP, Datta A, Bikson M, Su Y, Parra LC. Optimized multi-electrode stimulation increases focality and intensity at target. J Neural Eng 2011;8. https://doi.org/10.1088/1741-2560/8/4/046011. 046011.

[47] Windhoff M, Opitz A, Thielscher A. Electric field calculations in brain stimulation based on finite elements: an optimized processing pipeline for the generation and usage of accurate individual head models. Hum Brain Mapp 2013;34:923–35. https://doi.org/10.1002/hbm.21479.

[48] Antal A, Alekseichuk I, Bikson M, Brockmöller J, Brunoni AR, Chen R, et al. Low intensity transcranial electric stimulation: safety, ethical, legal regulatory and application guidelines. Clin Neurophysiol 2017;128:1774–809. https://doi.org/10.1016/j.clinph.2017.06.001.

[49] Oostenveld R, Fries P, Maris E, Schoffelen J-M. FieldTrip: open source software for advanced analysis of MEG, EEG, and invasive electrophysiological data. Comput Intell Neurosci 2011;2011:156869. https://doi.org/10.1155/2011/156869.

[50] Parra LC, Spence CD, Gerson AD, Sajda P. Recipes for the linear analysis of EEG. Neuroimage 2005;28:326–41. https://doi.org/10.1016/j.neuroimage.2005.05.032.

[51] Whitfield-Gabrieli S, Conn Nieto-Castanon A. A functional connectivity toolbox for correlated and anticorrelated brain networks. Brain Connect 2012;2:125–41. https://doi.org/10.1089/brain.2012.0073.

[52] Kamiński M, Ding M, Truccolo WA, Bressler SL. Evaluating causal relations in neural systems: Granger causality, directed transfer function and statistical assessment of significance. Biol Cybern 2001;85:145–57. https://doi.org/10.1007/s004220000235.

[53] O'Reilly JX, Woolrich MW, Behrens TEJ, Smith SM, Johansen-Berg H. Tools of the trade: psychophysiological interactions and functional connectivity. Soc Cogn Affect Neurosci 2012;7:604–9. https://doi.org/10.1093/scan/nss055.

[54] Henke K. A model for memory systems based on processing modes rather than consciousness. Nat Rev Neurosci 2010;11:523–32. https://doi.org/10.1038/nrn2850.

[55] Yonelinas AP, Ranganath C, Ekstrom AD, Wiltgen BJ. A contextual binding theory of episodic memory: systems consolidation reconsidered. Nat Rev Neurosci 2019;20:364–75. https://doi.org/10.1038/s41583-019-0150-4.

[56] Gomez J, Barnett MA, Natu V, Mezer A, Palomero-Gallagher N, Weiner KS, et al. Microstructural proliferation in human cortex is coupled with the development of face processing. Science 2017;355(80):68–71. https://doi.org/10.1126/science.aag0311.

[57] Grill-Spector K, Weiner KS, Kay K, Gomez J. The functional neuroanatomy of human face perception. Annu Rev Vis Sci 2017;3:167–96. https://doi.org/10.1146/annurev-vision-102016-061214.

[58] Wagner AD, Shannon BJ, Kahn I, Buckner RL. Parietal lobe contributions to episodic memory retrieval. Trends Cogn Sci 2005;9:445–53. https://doi.org/10.1016/j.tics.2005.07.001.
[59] Thut G, Miniussi C, Gross J. The functional importance of rhythmic activity in the brain. Curr Biol 2012;22:R658–63. https://doi.org/10.1016/j.cub.2012.06.061.
[60] Howard MW. Memory as perception of the past: compressed time in mind and brain. Trends Cogn Sci 2018;22:124–36. https://doi.org/10.1016/j.tics.2017.11.004.
[61] Folkerts S, Rutishauser U, Howard MW. Human episodic memory retrieval is accompanied by a neural contiguity effect. J Neurosci 2018;38:4200–11. https://doi.org/10.1523/JNEUROSCI.2312-17.2018.
[62] Ezzyat Y, Wanda PA, Levy DF, Kadel A, Aka A, Pedisich I, et al. Closed-loop stimulation of temporal cortex rescues functional networks and improves memory. Nat Commun 2018;9:365. https://doi.org/10.1038/s41467-017-02753-0.
[63] Ezzyat Y, Kragel JE, Burke JF, Levy DF, Lyalenko A, Wanda P, et al. Direct brain stimulation modulates encoding states and memory performance in humans. Curr Biol 2017;27:1251–8. https://doi.org/10.1016/j.cub.2017.03.028.
[64] Baird B, Smallwood J, Gorgolewski KJ, Margulies DS. Medial and lateral networks in anterior prefrontal cortex support metacognitive ability for memory and perception. J Neurosci 2013;33:16657–65. https://doi.org/10.1523/JNEUROSCI.0786-13.2013.
[65] Wolinski N, Cooper NR, Sauseng P, Romei V. The speed of parietal theta frequency drives visuospatial working memory capacity. PLoS Biol 2018;16:e2005348. https://doi.org/10.1371/journal.pbio.2005348.
[66] Opitz A, Falchier A, Yan C, Yeagle EM, Linn GS, Megevand P, et al. Spatiotemporal structure of intracranial electric fields induced by transcranial electric stimulation in humans and nonhuman primates. Sci Rep 2016;6:31236. https://doi.org/10.1038/srep31236.
[67] Alekseichuk I, Falchier AY, Linn G, Xu T, Milham MP, Schroeder CE, et al. Electric field dynamics in the brain during multi-electrode transcranial electric stimulation. Nat Commun 2019;10:2573. https://doi.org/10.1038/s41467-019-10581-7.
[68] Noury N, Hipp JF, Siegel M. Physiological processes non-linearly affect electrophysiological recordings during transcranial electric stimulation. Neuroimage 2016;140:99–109. https://doi.org/10.1016/j.neuroimage.2016.03.065.
[69] Neuling T, Ruhnau P, Weisz N, Herrmann CS, Demarchi G. Faith and oscillations recovered: on analyzing EEG/MEG signals during tACS. Neuroimage 2017;147:960–3. https://doi.org/10.1016/j.neuroimage.2016.11.022.
[70] Noury N, Siegel M. Analyzing EEG and MEG signals recorded during tES, a reply. Neuroimage 2018;167:53–61. https://doi.org/10.1016/j.neuroimage.2017.11.023.
[71] Kasten FH, Negahbani E, Fröhlich F, Herrmann CS. Non-linear transfer characteristics of stimulation and recording hardware account for spurious low-frequency artifacts during amplitude modulated transcranial alternating current stimulation (AM-tACS). Neuroimage 2018;179:134–43. https://doi.org/10.1016/j.neuroimage.2018.05.068.
[72] Reinhart RMG, Nguyen JA. Working memory revived in older adults by synchronizing rhythmic brain circuits. Nat Neurosci 2019. https://doi.org/10.1038/s41593-019-0371-x.